Progress in Natural Science: Materials International 26 (2016) 271–275

HOSTED BY

ELSEVIER

Contents lists available at ScienceDirect

Progress in Natural Science: Materials International

journal homepage: www.elsevier.com/locate/pnsmi

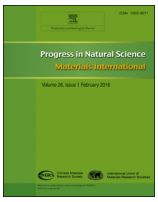

Original Research

NiO nanosheet assembles for supercapacitor electrode materials

Huanhao Xiao, Shunyu Yao, Hongda Liu, Fengyu Qu, Xu Zhang*, Xiang Wu*

College of Chemistry and Chemical Engineering, Harbin Normal University, Harbin 150025, China

ARTICLE INFO

Article history:
Received 30 March 2016
Accepted 20 April 2016
Available online 26 May 2016

Keywords:
NiO Nanosheets
Electrochemical
Supercapacitor electrode

ABSTRACT

In this paper, large scale hierarchically assembled NiO nanosheets have been favorably fabricated through a facile hydrothermal route. The as-prepared NiO nanosheet assembles were characterized in detail by various analytical techniques. The results showed these nanosheets present the thickness of about 30 nm and the surface area is 116.9 $m^2 g^{-1}$. These NiO nanosheet assembles were used as the working electrode materials in electrochemical tests, which demonstrated a specific capacitance value of 81.67 $F g^{-1}$ at the current density of 0.5 $A g^{-1}$ and excellent long cycle-life stability with 78.5% of its discharge specific capacitance retention after 3000 cycles at the current density of 0.5 $A g^{-1}$, revealing the as-synthesized NiO nanosheet assembles might be a promising electrode material for supercapacitor applications.

1. Introduction

In recent years, more and more pressing endeavors have been devoted to developing efficient energy storage and transform devices due to the increasing requirements for clean and renewable energy. Among them, because of the restrictive availability of fossil fuels and the increasing environmental pollutions, the electrochemical energy storage device has become more and more highlighted in future societies [1–4]. To be a kind of new-style electrochemical energy storage system, the supercapacitors have been extensively studied and considered to be one of the most promising green energy storage system due to their high efficiency and versatility [5]. The supercapacitors, also known as electrochemical capacitors, which reveal a set of features such as high power density, fast rates of charge-discharge, reliable cycling life and safe operation [6]. Based on the charge storage mechanism, they can be divided into two categories, electric double layer capacitors (EDLCs) and pseudocapacitors [7–10]. EDLCs store charges employing reversible adsorption of ions at the electrode and electrolyte interfaces. However, the pseudocapacitors store charges by redox reactions which occur on the surface of the electrode [11,12]. Obviously, pseudocapacitors exert higher energy density than EDLCs [13]. In particular, the pseudocapacitors usually supply higher specific capacitance than EDLCs because they rely on the reversible Faradic reactions occurring at the electrode surface [13–16]. In pseudocapacitors, electrons could be passed on to the valence bands of the anode reagent or the redox cathode [17]. Based on the traits of the pseudocapacitors, we know the properties of the pseudocapacitors are mainly rest upon the natures and structures of electrode materials [18,19].

Among various pseudocapacitor electrode materials, transition metal oxides with variable valencies are considered as ideal electrode materials for pseudocapacitors which could offer a variety of oxidation states for efficient redox charge transfer [20–25]. Amid transition metal oxides, NiO is one of the materials suitable for pseudocapacitor electrode applications. Lately, An et al. synthesized hierarchical NiO ultrafine nanowires grown on mesoporous NiO nanosheets by a facile and effective hydrothermal method [26]. Hu's group prepared flower-like NiO microspheres through a simple one-step hydrothermal process and investigated their supercapacitor performance [27]. In previous report, we prepared ultrathin NiO nanoflakes grown on nickel foam as supercapacitor electrode, NiO nanoflakes demonstrate the areal capacitance of 870 mF cm^{-2} at 1.0 mA cm^{-2} [28].

In this work, we utilize a facile and efficient self-assembly method to synthesize novel hierarchical porous NiO nanosheet assembles without using the assistant of any templates and surfactants at ambient temperature and pressure. These NiO nanosheets intermingle with each other and possess high surface area (116.9 $m^2 g^{-1}$). Electrochemical properties of the as-obtained product showed a specific capacitance of 81.76 $F g^{-1}$ with high rate capability and good cycling stability, which revealed NiO nanosheet assembles might be a promising electrode material for supercapacitor applications.

2. Experimental

NiO nanosheet assembles were prepared by a facile

* Corresponding authors.
E-mail addresses: xzhang@hrbnu.edu.cn (X. Zhang), wuxiang05@163.com (X. Wu).

Peer review under responsibility of Chinese Materials Research Society.

http://dx.doi.org/10.1016/j.pnsc.2016.05.007

hydrothermal process using easy available laboratory chemicals. All agentias are of analytical grade and were used without further purification. In a typical process, 3 mmol $NiSO_4 \cdot 6H_2O$ and 12 mmol $CO(NH_2)_2$ were dissolved in a 30 mL deionized water under vigorous stirring for 10 min to form a homogeneous solution. Then 2 mL ammonia was dropwise added into the mixed solution and stirred continuously for 30 min After that, the mixed solution was transferred into a 100 mL Teflon-lined stainless-steel autoclave and kept at 120 °C for 15 h. After completing the reaction, then the autoclave was cooled to room temperature naturally, and the obtained product was finally washed with deionized water and ethanol several times. Subsequently, the as-synthesized NiO product was dried at 60 °C in air for 6 h. Finally, the obtained product was annealed in a muffle kiln at 350 °C for 2 h.

The scanning electron microscope (SEM, Hitachi-4800), transmission electron microscope (TEM, JEOL-2010) were used to investigate the morphology and microstructure of the as-synthesized samples. The crystalline structure of the as-prepared products was characterized by using X-ray powder diffraction (XRD, Rigaku Dmax-rB, CuKα radiation, $\lambda = 0.1542$ nm, 40 kV,100 mA). The specific surface area of the as-synthesized product was estimated using the Brunauer-Emmett-Teller (BET) equation based on the nitrogen adsorption isotherm obtained with a Belsorp-max. The pore size distribution was determined by the Barrett-Joyner-Halenda (BJH) method that applied to the desorption branch of the adsorption-desorption isotherm.

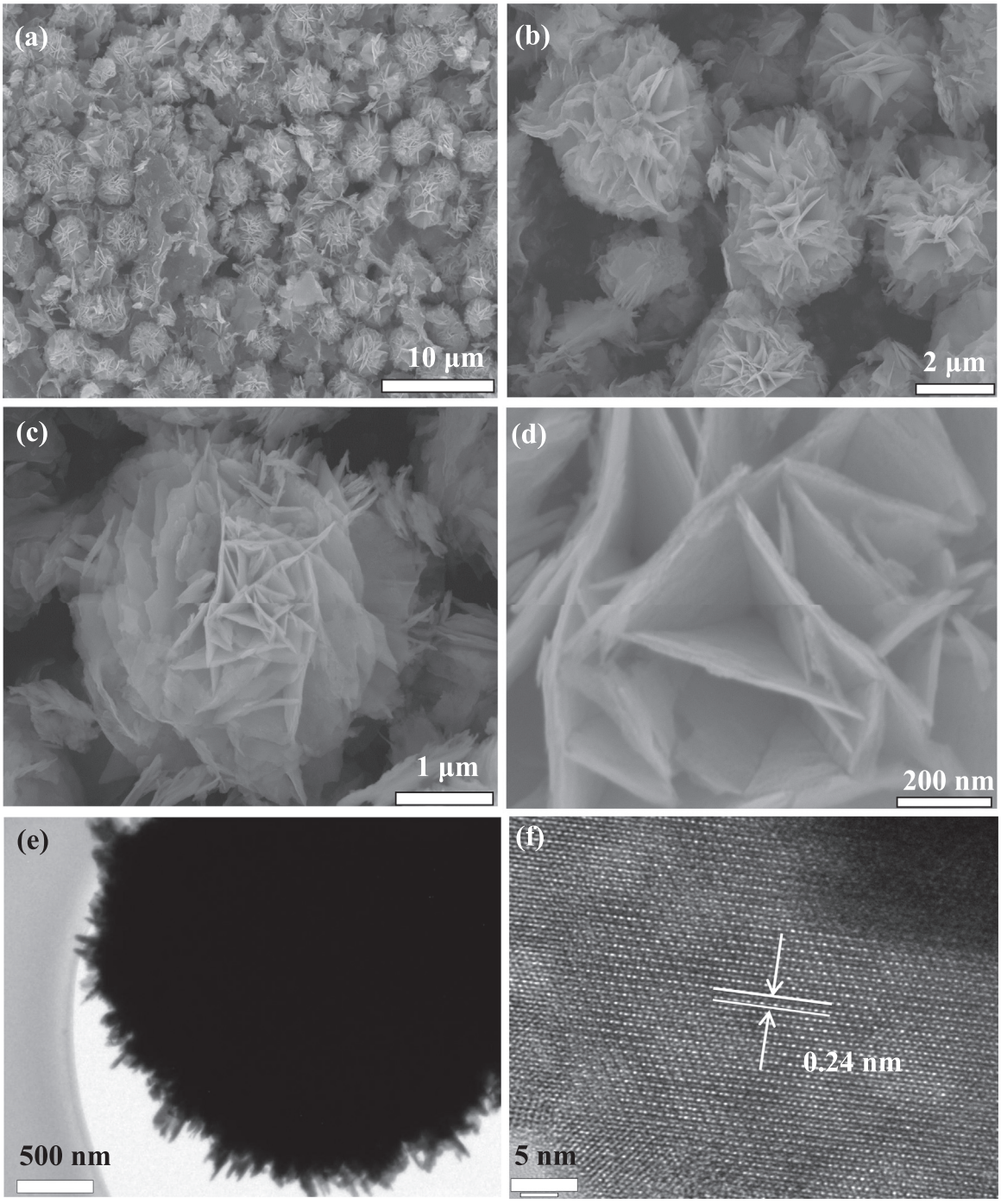

Fig. 1. (a-d) SEM images of the as- synthesized NiO products at different magnification (e-f) TEM image of the as- synthesized NiO products.

Electrochemical characteristics of the NiO nanosheet assembles were explored with cyclic voltammetry (CV), galvanostatic charge-discharge measurements, and electrochemical impedance spectroscopy (EIS) tests using a three-electrode electrochemical configuration in an electrochemical workstation (CHI660E, Shanghai, Chenhua). The as-obtained NiO products were used as the working electrode. Pt foil was used as the counter electrode and the Ag/AgCl as the reference electrode and 3 M KOH as the electrolyte. The working electrode was prepared by mixing 80 wt% NiO products, 15 wt% acetylene black, and 5 wt% polytetrafluoroethylene (PTFE) along with a few drops of ethanol. The suspending solution was coated onto nickel foam with an area of 1 cm^2. Finally, the as-obtained electrode was dried at 60 °C for 8 h. The electrode area is 1 cm^2, and the loading density is about 2.4 mg cm^{-2}. Cyclic voltammetry curves were measured in a potential range between −0.2 and 0.25 V at different scan rates, and the galvanostatic charge-discharge processes were performed by cycling the potential from −0.2 and 0.25 V at different current densities. The electrochemical impedance spectroscopy (EIS) measurements were performed by applying an AC voltage with 5 mV amplitude in the frequency range from 0.01 Hz to 100 kHz. The specific capacitance, C (F g^{-1}), of the electrode material was calculated from the galvanostatic discharge curves according to the following equation: $C = I\Delta t/(\Delta Vm)$. Where I is the discharge current(A), Δt is the discharge time(s), m is the mass of the active material(g), and ΔV is the voltage change (V) excluding IR drop in the discharge process.

3. Results and discussion

SEM was used first to examine the morphology and structure of the as-prepared product. Fig. 1(a)–(b) shows a typical low magnification SEM image, which shows a mass of hierarchical flower-shaped morphologies with pretty high density. Fig. 1(c)–(d) demonstrates different high magnification SEM images of NiO nanosheet assembles. As is shown in Fig. 1(d), it was easily observed that these hierarchical flower-shaped structures consist of ultrathin nanosheets which intermingle with each other. Meanwhile, the thickness of a single NiO nanosheet is about 30 nm. To get further structural information of NiO sample, the as-obtained product was analyzed by TEM. Fig. 1(e) shows low magnification TEM image of single NiO nanostructure consisting of many uniform-sized nanosheets, which manifests the full coherence with the observed SEM image in terms of shape and sizes. HRTEM image of single nanosheet in Fig. 1(f) shows the well-defined lattice fringes with the lattice spacing of 0.24 nm, which corresponds to the (111) lattice plane of bunsenite NiO structure.

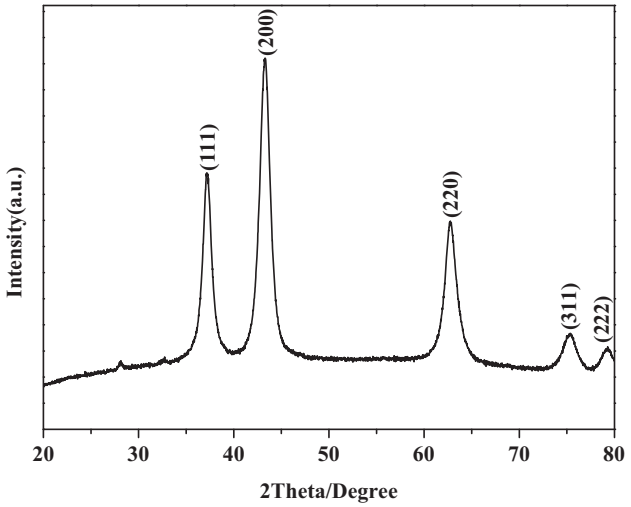

Fig. 2. Typical XRD pattern of the as- synthesized NiO products.

To further investigate the crystallinity and crystal phases of the NiO product, the prepared NiO nanosheet assembles were analyzed by X-ray diffraction. The result is shown in Fig. 2, all the diffraction peaks could be indexed to the bunsenite NiO structure by comparison with JCPDS Card No. 47–1049. No diffraction peaks of other impurities were found, revealing high purity of the as-synthesized NiO product. The sharp and strong peaks mean that the as-prepared sample is highly crystalline.

In order to confirm the specific surface area and pore size of NiO nanosheet assembles, the NiO product was tested by BET nitrogen adsorption-desorption measurements. Fig. 3(a) shows the nitrogen adsorption and desorption isotherms, revealing the isotherm of the as-synthesized NiO product possesses a type IV isotherm with a distinct hysteresis loop in the range of 0.2–1.0 P/P_0 on the basis of the IUPAC classification, indicating such a loop pertains to a mesoporous solid. The Brunauer-Emmett-Teller (BET) surface area value of the sample is calculated to be 116.9 m^2 g^{-1}. The pore size distribution of the sample calculated by desorption isotherm is shown in Fig. 3(b), indicating that a narrow pore size distribution peak is centered at about 3.066 nm, which further ascertains the mesoporous nature of NiO nanosheet assembles.

In order to study the pseudo-capacitive performance of the as-prepared material, the as-grown NiO nanosheet assembles was employed as the working electrode and tested using 3 M KOH as the electrolyte in a three-electrode configuration system. The results were showed in Fig. 4. For the sake of probing whether the pure nickel foam affects CV results of NiO product, CV curves of pure nickel foam and NiO nanosheet assembles active material were first tested at 40 mV s^{-1} and the results were shown in Fig. 4 (a). From the consequence, one can found that NiO nanosheet assembles electrode exhibits much higher capacitive current density than pure nickel foam, revealing that pure nickel foam devotes little to the total capacitance of NiO nanosheet assembles. CV curves of the working electrode collected at various scan rates ranging from 3 to 40 mV s^{-1} are shown in the potential range from −0.2 to 0.25 V to assess the rate dependent supercapacitive performance of the sample are shown in Fig. 4(b). From the CV curves in Fig. 4(b), we can observe that the capacitance is mainly on account of the redox reaction because the shape of the CV curves is distinguished from that of electric double-layer capacitance, which is normally close to an ideal rectangular, indicating that NiO nanosheet assembles electrode exhibits Faradic pseudo-capacitance behavior. The charge storage mechanism of NiO electrode may be caused by the following redox reaction [29,30].

$$NiO + zOH^- \text{—} zNiOOH + (1 - z)NiO + ze^- \quad (1)$$

From Fig. 4(b), we can find the area enclosed by the CV curves and the redox current increase with increasing scan rate and the shape of CV curve does not change very much even at a scan rate of 40 mV s^{-1}, revealing the good kinetic reversibility of NiO electrode. The galvanostatic charge-discharge test and cyclic behavior stability are tested by using the chronopotentiometry technique. Galvanostatic discharge tests were performed by using 3.0 M KOH as the electrolyte at different current densities from −0.2 to 0.25 V. Fig. 4(c) shows galvanostatic discharge curves of the sample at current densities of 0.5, 1.0, 1.2, 1.5, 2.0, and 3.0 A g^{-1}, respectively. As shown in the discharge curves, which represents very low IR drop, suggesting that NiO nanosheet assembles are good electrode materials in supercapacitors. Fig. 4 (d) demonstrates the calculated specific capacitance based on the discharge curves according to the above mentioned equation. The results were 81.76, 75.63, 73.66, 72.47, 70.6 and 64.72 F g^{-1} at

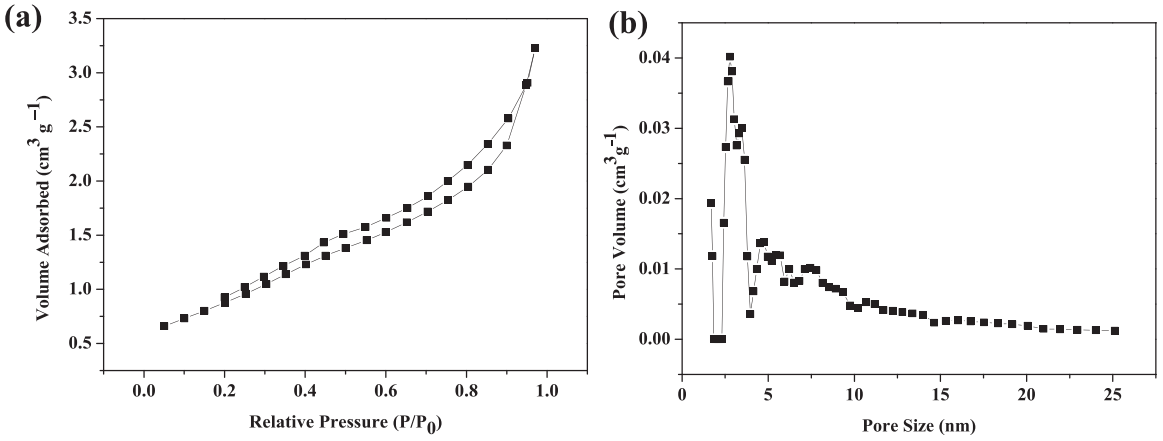

Fig. 3. (a) Nitrogen adsorption/desorption isotherm of the as- synthesized NiO products; (b) BJH pore size distribution plot of the as- synthesized NiO products.

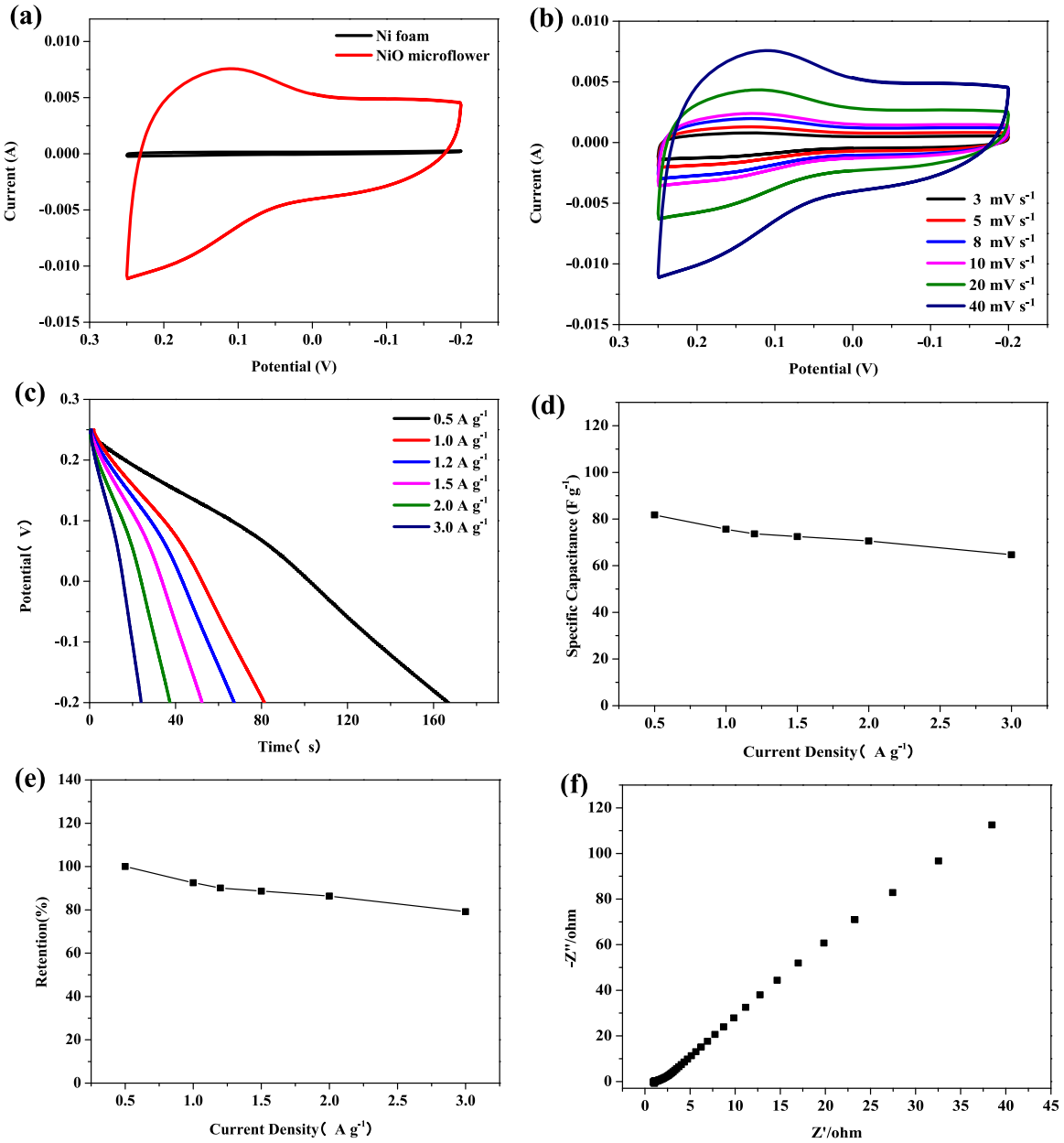

Fig. 4. Electrochemical tests of the as- synthesized NiO products (a) CV curves of pure nickel foam and NiO nanosheet assembles at a scan rate of 40 mV s^{-1}. (b) CV curves at scan rates between 3 and 40 mV s^{-1}. (c) discharge curves at current densities that ranged from 0.5 to 3 A g^{-1} (d) Current density dependence of the specific capacitance. (e) The capacitance retention ratio as a function of discharge current densities. (f) The EIS spectra of NiO nanosheet assembles electrode.

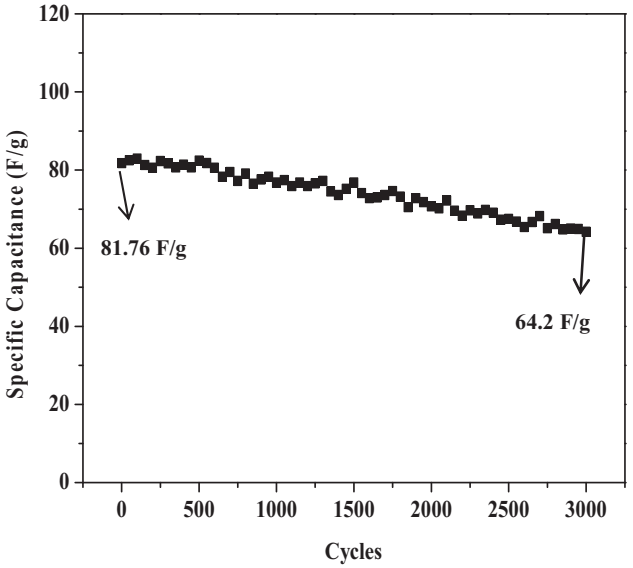

Fig. 5. Cycling stability of the NiO nanosheet assembles at a current density of 0.5 A g^{-1}.

current densities of 0.5, 1.0, 1.2, 1.5, 2.0, and 3.0 A g^{-1}, respectively, demonstrating that the specific capacitance decreases with increasing current density. As shown in Fig. 4(e), one can see NiO nanosheet assembles electrode retains 79.1% of its initial capacitance when the current density increases from 0.5 to 3.0 A g^{-1}, revealing the NiO electrode possesses a relatively high rate capability even at a current density of 3.0 A g^{-1}. To identify the resistive and capacitive element of the sample, Electrochemical impedance spectroscopy (EIS) was performed with a frequency range of 100 kHz to 0.01 Hz at an AC perturbation amplitude of 5 mV. Typical Nyquist plots of the electrodes are presented. Fig. 4 (f) shows the impedance of NiO nanosheet assembles electrode was found to be 1.2 Ω in the high frequency region, manifesting very low internal resistance of the electrode. It also further demonstrates NiO nanosheet assembles are excellent electrode materials for the supercapacitors.

Cycling stability is a crucial factor for the supercapacitor electrode performance. Stability of NiO nanosheet assembles as an electrode material was evaluated by repeating continuous galvanostatic charge-discharge measurements at a current density of 0.5 A g^{-1} for 3000 cycles. The results were showed in Fig. 5, galvanostatic charge-discharge cycles of NiO nanosheet assembles electrode retain about 78.5% of the initial specific capacitance after 3000 cycles, indicating its excellent long-term cycling stability. The high capacitance retention implies that the as-synthesized NiO nanosheet assembles are suitable materials for supercapacitor applications.

4. Conclusions

In summary, NiO nanosheet assembles have been successfully synthesized via a facile hydrothermal process at low temperature in the absence of any surfactants. The as-synthesized products consisted of two dimensional nanosheets with the thicknesses of about 30 nm and high BET surface area (116.9 m^2 $g^{-1)}$ and mesoporous structure. The electrochemical properties of as-synthesized products shows specific capacitance of 81.76 F g^{-1} at discharge current densities of 1 A g^{-1} and excellent cycling stability (retain 78.5% after 3000 cycles at 0.5 A g^{-1}), indicating their excellent electrochemical performance and good cycling stability. The electrochemical performance can make the hierarchical NiO structures to be one of the prospective electrode materials for electrochemical energy storage applications.

Acknowledgement

This work was supported by the Scientific Research Fund of Heilongjiang Provincial Education Department (12531179).

References

[1] G.H. Zhang, T.H. Wang, X.Z. Yu, H. Zhang, H.G. Duan, B.G. Lu, Nano Energy 2 (2013) 586.
[2] Y.T. Han, X. Wu, Y.L. Ma, L.H. Gong, F.Y. Qu, H.J. Fan, CrystEngComm 13 (2011) 3506.
[3] L.Q. Mai, X.C. Tian, X. Xu, L. Chang, L. Xu, Chem. Rev. 114 (2014) 11828.
[4] L.J. Xie, K.X. Li, G.H. Sun, Z.G. Hu, C.M. Zhang, J. Solid State Electrochem. 17 (2013) 55.
[5] X.H. Xia, Y.Q. Zhang, D.L. Chao, C. Guan, Y.J. Zhang, L. Li, X. Ge, I. Bacho, J.P. Tu, H.J. Fan, Nanoscale 6 (2014) 5008.
[6] K.L. Van, T.T.L. Thi, Progress Nat. Sci.: Mater. Int. 24 (2014) 191.
[7] P. Simon, Y. Gogotsi, Nat. Mater. 7 (2008) 845.
[8] R.R. Salunkhe, Y.H. Lee, K.H. Chang, J.M. Li, P. Simon, J. Tang, N.L. Torad, C.C. Hu, Y. Yamauchi, Chem. Eur. J. 20 (2014) 13838.
[9] M. Rajkumar, C.T. Hsu, T.H. Wu, M.G. Chen, C.C. Hu, Progress Nat. Sci.: Mater. Int. 25 (2015) 527.
[10] Q. Yang, Z.Y. Lu, J.F. Liu, X.D. Lei, Z. Chang, L. Luo, X.M. Sun, Progress Nat. Sci.: Mater. Int. 23 (2013) 351.
[11] A.K. Shukla, S. Sampath, K. Vijayamohan, Curr. Sci. 79 (2000) 1656.
[12] G.Z. Chen, Progress Nat. Sci.: Mater. Int. 23 (2013) 245.
[13] B. Wang, T. Zhu, H.B. Wu, R. Xu, J.S. Chen, X.W. Lou, Nanoscale 4 (2012) 2145.
[14] C. Guan, X.L. Li, Z.L. Wang, X.H. Cao, C. Soci, H. Zhang, H.J. Fan, Adv. Mater. 24 (2012) 4186.
[15] Y.G. Wang, H.Q. Li, Y.Y. Xia, Adv. Mater. 18 (2006) 2619.
[16] G.A. Snook, P. Kao, A.S. Best, J. Power Sources 196 (2011) 1.
[17] Q.F. Wang, B. Liu, X.F. Wang, S.H. Ran, L.M. Wang, D. Chen, G.Z. Shen, J. Mater. Chem. 22 (2012) 21647.
[18] G.P. Wang, L. Zhang, J.J. Zhang, Chem. Soc. Rev. 41 (2012) 797.
[19] B.S. Yin, S.W. Zhang, Y. Liu, Y. Jiao, F.Y. Qu, X. Wu, CrystEngComm 16 (2014) 9999.
[20] P. Yang, X. Xiao, Y. Li, Y. Ding, P. Qiang, X. Tan, W. Mai, Z. Lin, W. Wu, T. Li, H. Jin, P. Liu, J. Zhou, C.P. Wong, Z.L. Wang, ACS Nano 7 (2013) 2617.
[21] Y. Liu, D. Yan, R. Zhuo, S. Li, Z. Wu, J. Wang, P. Ren, P. Yan, Z. Geng, J. Power Sources 242 (2013) 78.
[22] P. Lu, F. Liu, D. Xue, H. Yang, Y. Liu, Electrochim. Acta 78 (2012) 1.
[23] Y. Zhang, C. Sun, P. Lu, K. Li, S. Song, D. Xue, CrystEngComm 14 (2012) 5892.
[24] Y. Jiao, Y. Liu, B.S. Yin, S.W. Zhang, F.Y. Qu, X. Wu, Nano Energy 10 (2014) 90.
[25] B.S. Yin, S.W. Zhang, H. Jiang, F.Y. Qu, X. Wu, J. Mater. Chem. A 3 (2015) 5722.
[26] L. An, K.B. Xu, W.Y. Li, Q. Liu, B. Li, R.Z. Zou, Z.G. Chen, J.Q. Hu, J. Mater. Chem. A 2 (2014) 12799.
[27] Q.F. Wu, Y.F. Liu, Z.H. Hu, J. Solid State Electrochem. 17 (2013) 1711.
[28] H.H. Xiao, F.Y. Qu, X. Wu, Appl. Surf. Sci. 360 (2016) 8.
[29] B. Ren, M.Q. Fan, Q. Liu, J. Wang, D.L. Song, X.F. Bai, Electrochim. Acta 92 (2013) 197.
[30] M. Khairy, S.A. El-Safty, RSC Adv. 3 (2013) 23801.